Restoring Force Model For A New Type of Bolted Prefabricated Beam-To-Column Joint

Jiang Haotian
Jinling Institute of Technology
Miao Hailin
Jinling Institute of Technology
Jin Chenhua
Jinling Institute of Technology
LI Qingning
Xi'an University of Architecture and Technology
Yan Lei (458691102@qq.com)
Chongqing Three Gorges University

Research Article

Keywords: restoring force model, steel-encased concrete column, failure mode, prefabricated beam-to-column joint

Posted Date: June 21st, 2021

DOI: https://doi.org/10.21203/rs.3.rs-599485/v1

Abstract

The wet prefabricated beam-to-column joint (PBCJ) has a densely reinforced panel zone and is difficult to construct, leading to poor connection reliability. To address this problem, we propose a dry PBCJ, where the concrete column is encased with steel plates at the connection and the beams and the column are connected by high-strength bolts. The method for constructing the joint is described herein. A total of six full-scale PBCJs were designed and subjected to quasi-static loading tests with different stirrup ratios, reinforcement strengths, and joint strengthening methods. Based on the test loading process, the joint failure mode is summarised, and a trilinear backbone curve model is proposed. According to the characteristics of the hysteresis curve and the backbone curve, the stiffness degradation law and hysteresis rule are analysed; then, the restoring force model for the new type of PBCJ is established, and the model results are compared with the test results. The data show that the new bolted PBCJ undergoes the cracking, yielding, ultimate, and failure stages; the trilinear backbone curve, which is composed of an elastic section, an elastoplastic section, and a plastic section, well describes the load-carrying characteristics of the joint. The backbone curve calculated by the established restoring force model is consistent with that obtained from the tests, indicating that the model can accurately describe the energy dissipation performance of the new PBCJ and thus provide a theoretical basis for the seismic performance analysis of this type of joint.

Introduction

To date, numerous efforts have been devoted to the study of restoring force models and the corresponding characteristic parameters of basic reinforced concrete members and joints, accompanied by the proposed calculation equations, while little research has been carried out on the restoring force models of prefabricated beam-to-column joints (PBCJs) [1–3]. When responding to large earthquakes, structures may enter an elastoplastic state, for which an elastic analysis is no longer applicable [4–7]. To understand the entire process of the dynamic load-carrying behaviour of PBCJs under large earthquakes, it is necessary to have an accurate constitutive expression for the material or cross-section under reversal loading [8,9], that is, the curve of the relationship between the restoring force and the deformation. In addition, the mechanical properties (e.g., stiffness, strength, ductility, and energy dissipation capacity) of PBCJs can be derived from the restoring force model, forming an important basis for the elastoplastic dynamic analysis of prefabricated structures. However, the actual restoring force curves of PBCJs are complex and difficult to apply directly in the seismic analysis of engineering structures. Therefore, it is particularly important to have a practically applicable and mathematically simple restoring force curve for the new type of bolted PBCJ [9,10].

Joint Design And Fabrication

2.1 Joint design

The proposed new type of bolted PBCJ is composed of a prefabricated concrete column, end-strengthened reinforced concrete beams, high-strength bolts and prestressing tendons. The design dimensions of the joint are shown in Fig. 1.

A total of six PBCJs (PAN-03 to -08) were designed in this study. The column had a concrete strength grade of C60, cross-sectional dimensions of 400 mm × 400 mm, and a stirrup spacing of 30 (50) mm. The panel zone of the joint was encased with 4 mm-thick steel plates. Except for those of specimen PAN-03, the column end plates of each of the other PAN-series specimens were welded together on both sides from outside using steel plate strips. The specimen PAN-07 (08) was encased with 4-mm-thick steel plates within a range of 450 mm from the beam end to ensure that concrete would not spall when it entered the plastic stage; additionally, after the specimen reached the ultimate load-carrying capacity, the material ductility could be given full play, thereby significantly improving the seismic performance of the PBCJ.

2.2 Joint fabrication

The method for fabricating and assembling the bolted PBCJs is the following. The PBCJs were fabricated by others in workshops using high-strength compound stirrups; the reinforcement cages of beams and columns were fabricated separately, as shown in Fig. 2.

The prestressing tendons in the beams and the high-strength bolts used for the bolted joints were inserted into polyvinyl chloride (PVC) pipes at the appropriate positions before casting the concrete to ensure the accuracy of the PBCJ assembly at a later stage. The concrete of the precast beam was cast vertically. A 20-mm splicing gap was reserved between the beams and the columns to ensure the verticality of the PBCJ. After the PBCJ was assembled, beams and columns were adjusted to ensure their verticality and place them in the same plane so as to improve the accuracy and seismic performance of the PBCJ. The 20-mm gap was filled with high-strength non-shrinking grout. After the grout reached 75% of the strength, the high-strength bolts were pretensioned to provide a strong joint.

Test Overview

3.1 Material property test

A uniaxial tensile test was performed on the steel used in this study to determine its yield strength, tensile strength, modulus of elasticity, and elongation. The mechanical properties of the steel are shown in Table 1.

Table 1 Mechanical properties of steel

Steel specification	Yield strength	Ultimate strength	Modulus of elasticity	Elongation
4	296.7	448.3	2.03×10^5	29
5	1157.51	1776.7	2.00×10^5	1.2
18	451.7	688.3	2.10×10^5	23.5
22	698.3	878.3	2.11×10^5	21
25	1026.67	1161.2	2.06×10^5	17

3.2 Loading protocol

According to the ”Specification of testing methods for earthquake resistant buildings” [11], when a specimen was in the elastic stage, the loading was force-controlled, with the loading applied at increments of 30 kN level by level; when the regular reinforcement of the specimen entered the yielding stage, the loading was displacement-controlled with different levels of loading corresponding to different multiples of the yield displacement. The loading was cyclically reversed three times at each level. The loading process continued until the specimen failed or its load-carrying capacity decreased to approximately 85% of the ultimate load [11]. The loading setup is shown in Fig. 3.

Analysis Of Failure Characteristics

Low-cycle reversed loading was applied on the six PBCJs, and the test phenomena were observed and recorded. On this basis, the loading stage can be divided into the cracking, yielding, ultimate and failure stages.

The cracking stage: At the initial stage of loading, as a PBCJ was subjected to the cyclic load reversal, vertical flexural cracks appeared at both upper and lower flanges of the beam end with basically the same the crack development. Additionally, the cracking load of the PBCJ increased due to the prestressing effect, and minor inclined cracks appeared in the beam web with the increased load.

The yielding stage: After the PBCJ yielded, the loading was displacement-controlled. When the displacement reached 2Δ, the inclined crack in the beam web was 0.4 mm wide; when the displacement further increased to 3Δ, there was a sign of disengagement of the connecting end plates of the PBCJ from both upper and lower flanges, the inclined crack widened to 0.5 mm, and the steel jackets of PAN-07 and − 08 slipped slightly.

The ultimate stage: When the displacement reached 4Δ, both the number and width of cracks remained basically unchanged with the increase in load, the deformation mainly occurred at the interface between the connecting end plates and the beam-end steel jackets in the panel zone of the PBCJ, and the plastic hinge was formed at this interface.

The failure stage: The load-carrying capacity exhibited a decreasing trend, the concrete in the plastic hinge region was crushed, characteristic flexural-shear failure occurred in the beam, the concrete cover spalled, and the connecting end plates of the PBCJ warped slightly.

The failure modes of all six specimens were basically the same. The failure was mainly concentrated in the plastic hinge region within a certain range from the beam end, where the concrete was crushed and spalled; the high-strength bolts yielded during the loading process; the precast concrete columns were intact, and the specimens failed primarily in flexure-shear at beam ends, a failure mode in line with the strong-column-weak-beam design concept. Figure 4 shows the failure characteristics of the new type of bolted PBCJ.

Backbone Curves

5.1 Backbone curve analysis

The backbone curves obtained from the tests were modelled using numerical fitting [10]. The dimensionless backbone curves are shown in Fig. 5.

By analysing the trend of the dimensionless backbone curves, the load-carrying and deformation characteristics of the PBCJ are roughly divided into three stages:

(1) The elastic stage: Before the PBCJ entered the elastoplastic state, the load-displacement curve was basically linear, and only a few tiny cracks were generated. At this stage, the slope of the curve was the initial stiffness of the PBCJ, and the prefabricated beam-to-column subassemblage was basically in an elastic state.

(2) The strengthening stage: After the PBCJ entered the elastoplastic stage, as the displacement increased, the load growth rate decreased and the stiffness degraded severely. This is mainly because as the PBCJ yielded, the cracks at the beam ends propagated continuously, causing the accumulation of damage to concrete.

(3) The degradation stage: After the PBCJ entered the plastic stage, the load and displacement were negatively correlated. The concrete in the plastic hinge region of the panel zone of the PBCJ was crushed. When the load degraded to 85% of the ultimate load, the loading was stopped.

By summarising the three stages that reflect the basic change trend of the backbone curves, the characteristics of the load-carrying and deformation process of the specimens can be visually observed.

5.2 Backbone curve model

Based on the analysis of the test results, an asymmetric trilinear model with descending sections in both positive and reverse directions was used to fit the backbone curves of the PBCJ specimens. A three-segment polyline was obtained by fitting the dimensionless data of the specimens using the yield point,

the ultimate load point, and the maximum deformation point as the boundary points [9]. Three points in each direction were determined from the fitted three-segment polyline: the yield point (0.38, 0.88), the ultimate load point (1.0, 1.0) and the maximum deformation point (1.41, 0.9) in the positive direction; and the yield point (-0.375, -0.84), ultimate load point (-1.0, -1.0) and maximum deformation point (-1.30, -0.88) in the negative direction. It is noted that the maximum displacement was the average of the ultimate displacements of different specimens. The fitting equations are provided in Table 2.

Table 2
Backbone curve fitting equations

Line segment	Fitting equation
OA	$P/P_u^+=2.314\Delta/\Delta_u^+$
AB	$P/P_u^+=0.205\Delta/\Delta_u^+ + 0.802$
BC	$P/P_u^+=-0.056\Delta/\Delta_u^+ + 1.028$
OD	$P/P_u^-=2.236\Delta/\Delta_u^-$
DE	$P/P_u^-=0.267\Delta/\Delta_u^--0.745$
EF	$P/P_u^-=-0.234\Delta/\Delta_u^--1.215$

5.3 Backbone curve verification

Using the regression equation of each stage of the backbone curve model and the coordinates of the characteristic points given in Table 2, the theoretical backbone curve of the PBCJ was calculated and then compared with the test result of each PBCJ specimen, as shown in Fig. 6. The data in the figure show that the proposed trilinear backbone curve model is consistent with the test values of the joints and thus well reflects the load-displacement relationship of this type of joint under the quasi-static loading test.

5.4 Analysis of hysteresis curve test results

The red dashed lines in Fig. 9 are the hysteresis curves of the six specimens obtained from the tests. These curves show that:

(1) The hysteresis curves obtained from the new type of bolted PBCJ are full, basically without pinching, and roughly in a parallelogram shape. The positive and reverse stiffnesses of the PBCJs are similar.

(2) With the increase of the horizontal load at the end of the column, minor vertical cracks appeared in the concrete at both upper and lower flanges of the beam in the plastic hinge region, and the area enclosed

by the hysteresis curve is very small. After the longitudinal regular reinforcement yielded, the hysteresis curve of the PBCJ is full and spindle-shaped.

(3) At the ultimate load, the concrete cover in the plastic hinge region spalled severely and some stirrups were exposed; however, the load-carrying capacity of the PBCJ decreased slowly after the peak load was reached. It is thus concluded that the PBCJ can still carry the corresponding load after the concrete cover spalls, demonstrating good seismic performance.

5.5 Stiffness degradation law

(1) Degeneration law of the positive unloading stiffness K_1

The relation between $K_i / K_0^{\pm}$ and $\Delta_i / \Delta_u^{\pm}$ is calculated by regression analysis, as shown in Fig. 7.

After the yielding of the PBCJ, the slope of the section of the curve from the starting point of positive unloading to the point at which the force is zero on the hysteresis loop, as obtained from the regression analysis, is the positive unloading stiffness [8] K_1. The regression equation for this section of the stiffness degradation curve is as follows:

$$K_1 / K_0^+ = -0.3659 \ln\left(\Delta_1 / \Delta_u^+\right) + 0.6348 \qquad (5\text{-}1)$$

(2) Degeneration law of the reverse unloading stiffness K_2

The slope of the section of the curve from the point at which the positive unloading becomes zero to the point at which the reverse loading reaches the peak under the same cyclic load, as obtained from the regression analysis, is the reverse loading stiffness [8] K_2. The regression equation for this section of the stiffness degradation curve is as follows:

$$K_2 / K_0^- = -0.2983 \ln\left(\Delta_2 / \Delta_u^+\right) + 0.0608 \qquad (5\text{-}2)$$

(3) Degeneration law of the negative unloading stiffness K_3

Under the same cyclic loading, the slope of the section of the curve from the starting point of reverse unloading to the point at which the force is unloaded to zero, as obtained from the regression analysis, is the reverse loading stiffness [8] K_3. The regression equation for this section of the stiffness degradation curve is as follows :

$$K_3 / K_0^- = -0.4670 \ln\left(\Delta_3 / \Delta_u^-\right) + 0.5372 \qquad (5\text{-}3)$$

(4) Degeneration law of the positive loading stiffness K_4

Under the same cyclic loading, the slope of the section of the curve from the point at which the reverse unloading reaches zero to the point at which the positive loading reaches the peak, as obtained from the

regression analysis, is the positive loading stiffness [8] K_4. The regression equation for this section of the stiffness degradation curve is as follows:

$$K_4 / K_0^+ = -0.2627\ln\left(\Delta_4 / \Delta_u^-\right) + 0.0259 \qquad (5\text{-}4)$$

where K_0^+ and K_0^- are the initial stiffnesses corresponding to positive and reverse loading, respectively; Δ_u^+ and Δ_u^- are the displacements corresponding to the maximum positive and reverse loading, respectively; and Δ_1, Δ_2, Δ_3, and Δ_4 are the displacements under positive unloading, displacement after positive unloading, displacement under reverse unloading, and displacement after reverse unloading, respectively.

5.6 Hysteresis rule

The fitted trilinear backbone curve agrees well with the stiffness degradation law, and thus the hysteresis rule applicable to this type of joint is proposed, as shown in Fig. 8.

(1) In the OA and OD sections, the structural member is in the elastic state, where there is a linear load-displacement relationship. The positive and reverse loading and unloading stiffnesses are the initial stiffnesses.

(2) In the AB and DE sections, the structural member enters the yielding stage, and its loading and unloading stiffnesses at all levels gradually decrease. The unloading [8] starts at point *a* towards point *b*, with an unloading stiffness K_{ab}; then, the reverse loading is directed towards point *c*, with a loading stiffness K_{bc}; finally, the reverse unloading is directed towards point *d*, with an unloading stiffness K_{cd}.

(3) The positive loading is directed towards point *a*, with a loading stiffness K_{da}; the positive loading continues along the backbone curve described by the equations in Table 2 and starts the next cycle of displacement-controlled loading.

5.7 Verification of the restoring force model for the new type of PBCJ

The seismic performance of the new type of bolted PBCJ is affected by various parameters that defy the establishment of a unified equation to accurately describe the load-displacement relationship of the joint. High regularity can be attained from the backbone curve and the stiffness degradation curve, thereby proving the reasonableness of the restoring force model of the new type of bolted PBCJ. Figure 9 compares the hysteresis curve constructed according to the above stiffness degradation and hysteresis rules with the hysteresis curves obtained from the tests. Evidently, the proposed restoring force model has a high goodness of fit, and the discrepancies in the calculation results for some individual members were mainly due to the dispersion of the backbone curves after nondimensionalisation. The overall results

were very good, proving that the proposed restoring force model can accurately simulate the seismic performance of this type of joint.

Conclusions

(1) The performance of the proposed new type of bolted prefabricated beam-to-column joint during the entire test process was divided into cracking, yielding, ultimate and failure stages. The first crack appeared when the load reached 120 kN, the specimen entered the yielding stage when the load was 210 kN and the concrete in the plastic hinge region was crushed after the ultimate load was reached.

(2) The dimensionless backbone curve has good consistency, and the proposed trilinear backbone curve model is in good agreement with the test results.

(3) On the basis of the backbone curve model, the calculation method for the loading and unloading stiffnesses is determined, and the unified calculation equations for loading and unloading stiffnesses are obtained. A restoring force model is proposed by combining the stiffness degradation law and the backbone curve model of the joint. The theoretical values of the hysteresis curve agree well with the test values. The proposed restoring force model enables the elastoplastic analysis and seismic design of structures with this type of joint under large earthquakes.

References

[1] Li C, Zhou Z, Xie Q. Hysteretic performance analysis of self-centering beam-column connections with SMA bars and friction energy dissipator [J]. Engineering Mechanics, 2018, 35(4): 115-123.

[2] Cao X, Feng D, Wang Z, Wu G. Investigation on modelling approaches for prefabricated concrete beam-to-column connections using openSEES [J]. China Civil Engineering Journal, 2019, 52(4): 13-27.

[3] Liu Y, Guo Z, Lv Y, Huang Q, Wang Z. Experimental study on seismic behavior of full-scale PRC columns with new mechanical splice technique for longitudinal reinforcement [J]. Journal of Building Structures, 2017, 11: 101-110.

[4] GUAN D，GUO Z，XIAO Q，et al，Experimental study of a new beam-to-column connection for precast concrete frames under reversal cyclic loading [J]，Advances in Structural Engineering，2016，19，3，: 529-545，

[5] Cai J, Feng J, Wang Z, Zhu H. Seismic behavior of frame comprised of precast prestressed concrete components [J]，Acta Scientiarum Naturalium Universitatis Sunyatseni, 2009, 48(2): 136-140.

[6] Zhao P. Restoring force modelling of precast prestressed concrete frame beam-column joints [J]. Earthquake Resistant Engineering and Retrofitting, 2016.

[7] NAKAKI S D,ENGLEKIRK R E,PLAEHN J L, et al□Ductile Connectors for a Precast Concrete Frame [J]. PCI Journal,1994□4□□46-58□

[8] Chen Y, Chen C. Study on restoring force model of prefabricated self-centering rocking steel moment-resisting frame [J]. Journal of Building Structures, 2020.

[9] Wu G, Feng D. Research progress on fundamental performance of precast concrete frame beam-to-column connections [J]. Journal of Building Structures, 2018, 2, 1-16.

[10] Guo T, Song L, Zhang G, Gu Y. Experimental study on beam-column connections of self-centering prestressed concrete frame with web friction devices [J]. China Civil Engineering Journal, 2012, 45(6): 23-32.

[11] JGJ101-96. Specification of testing methods for earthquake resistant buildings [S]. Beijing: Research Institute of Standards and Norms, Ministry of Housing and Urban-Rural Development, China, 1997.

Figures

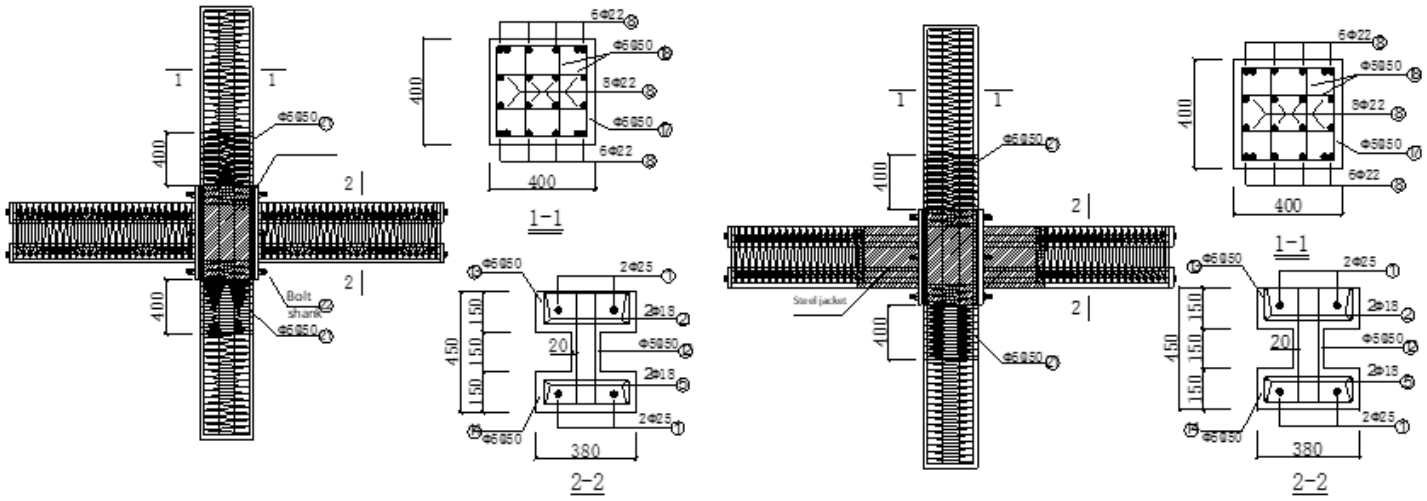

Figure 1

Detailed dimensions of the joint

Figure 2

Reinforcement cages

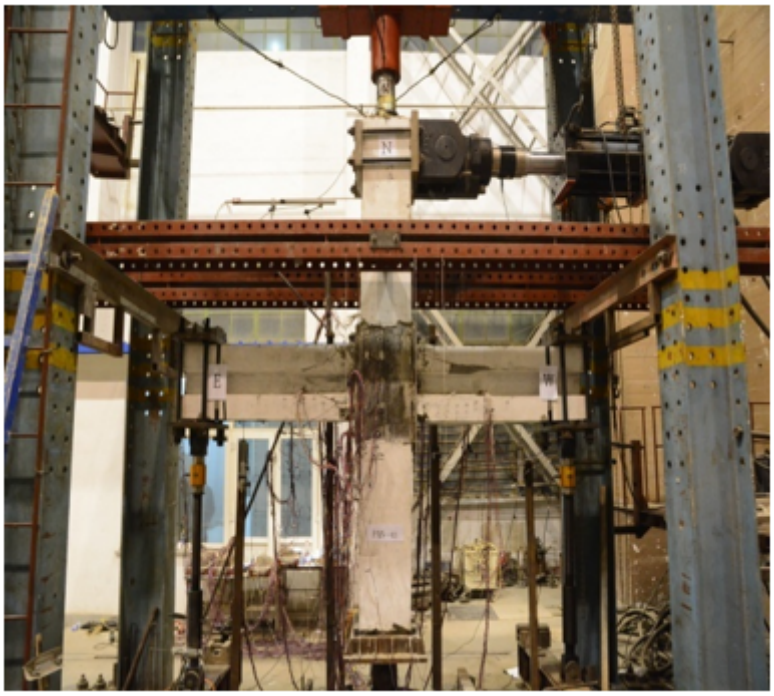

Figure 3

The loading setup

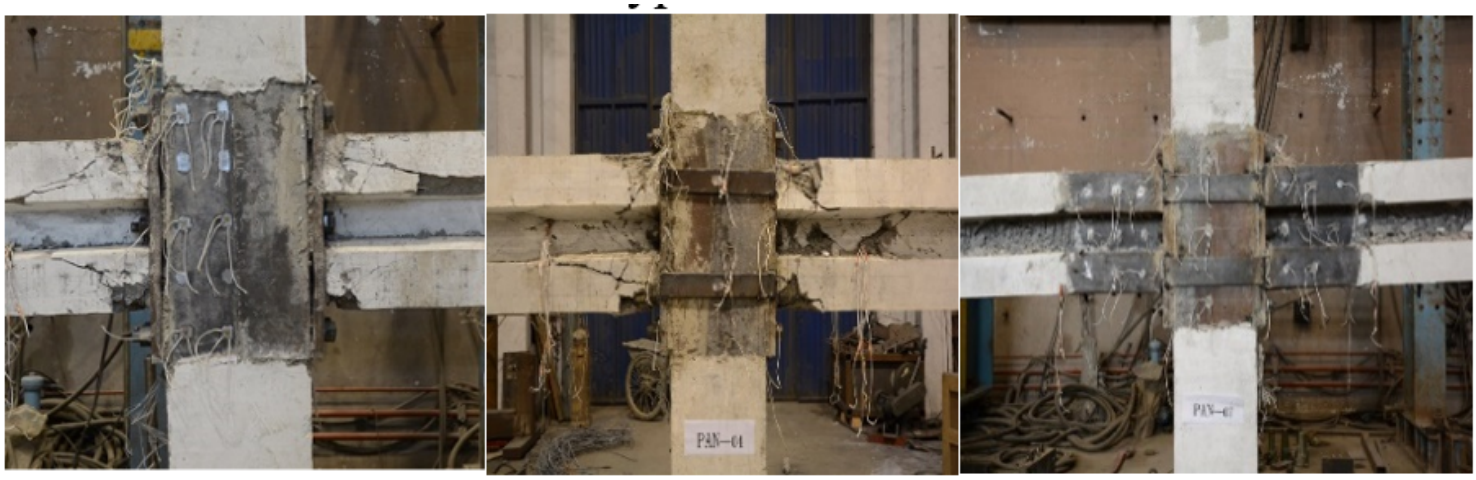

Figure 4

Joint failure characteristics

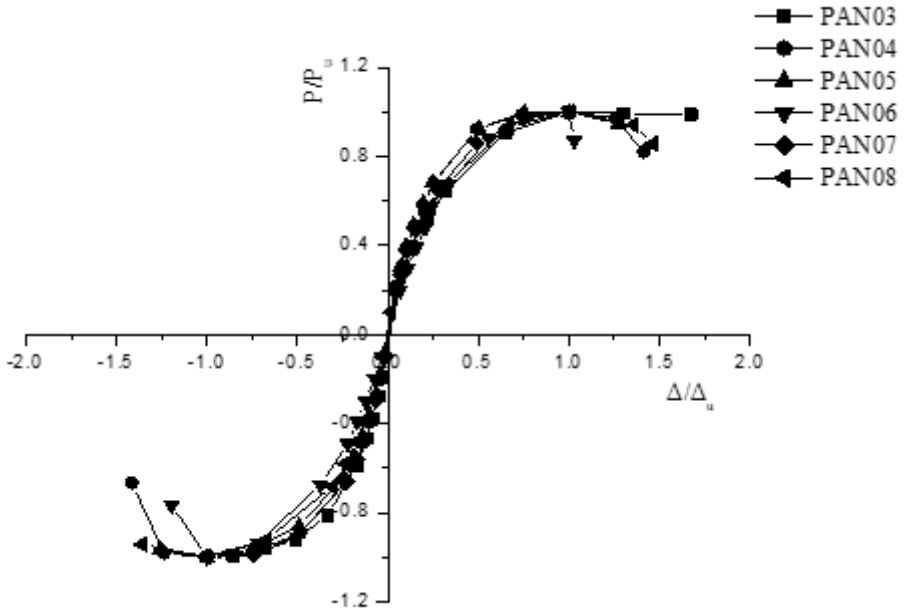

Figure 5

Dimensionless backbone curves

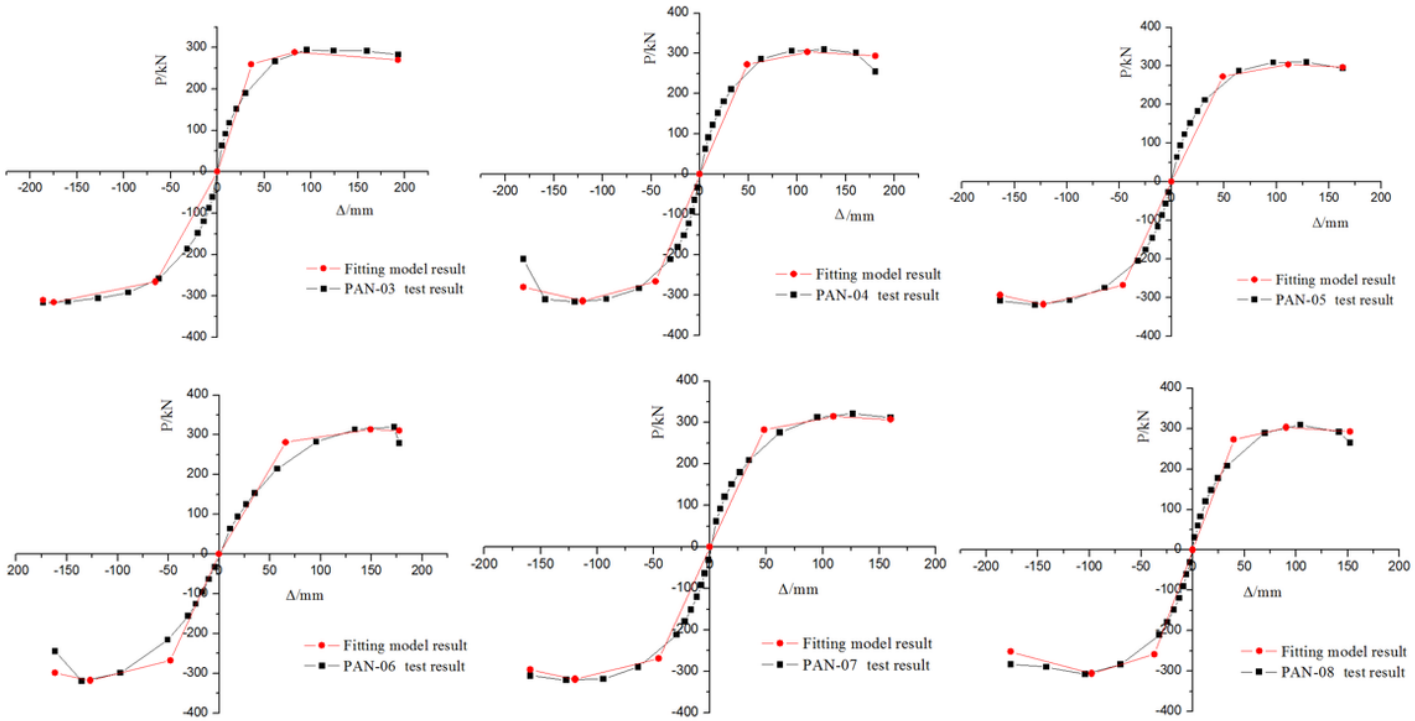

Figure 6

Comparison of backbone curves

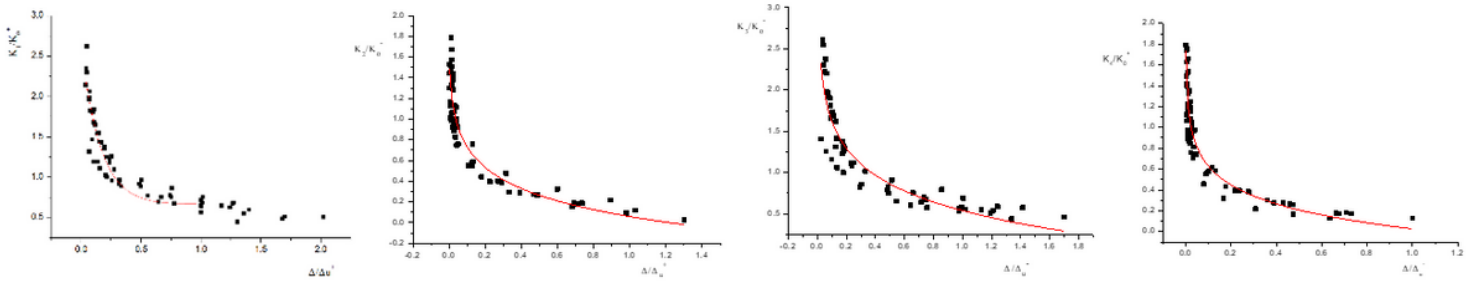

Figure 7

Regression curves

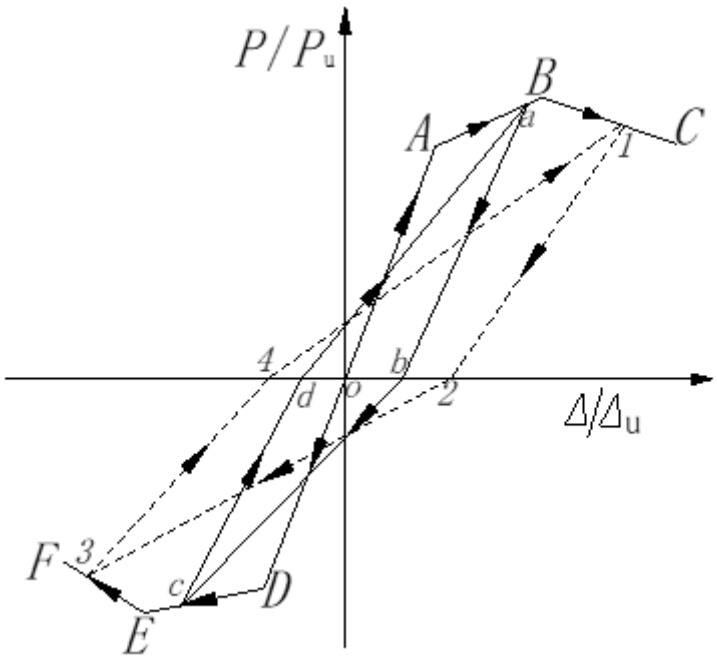

Figure 8

The hysteresis rule

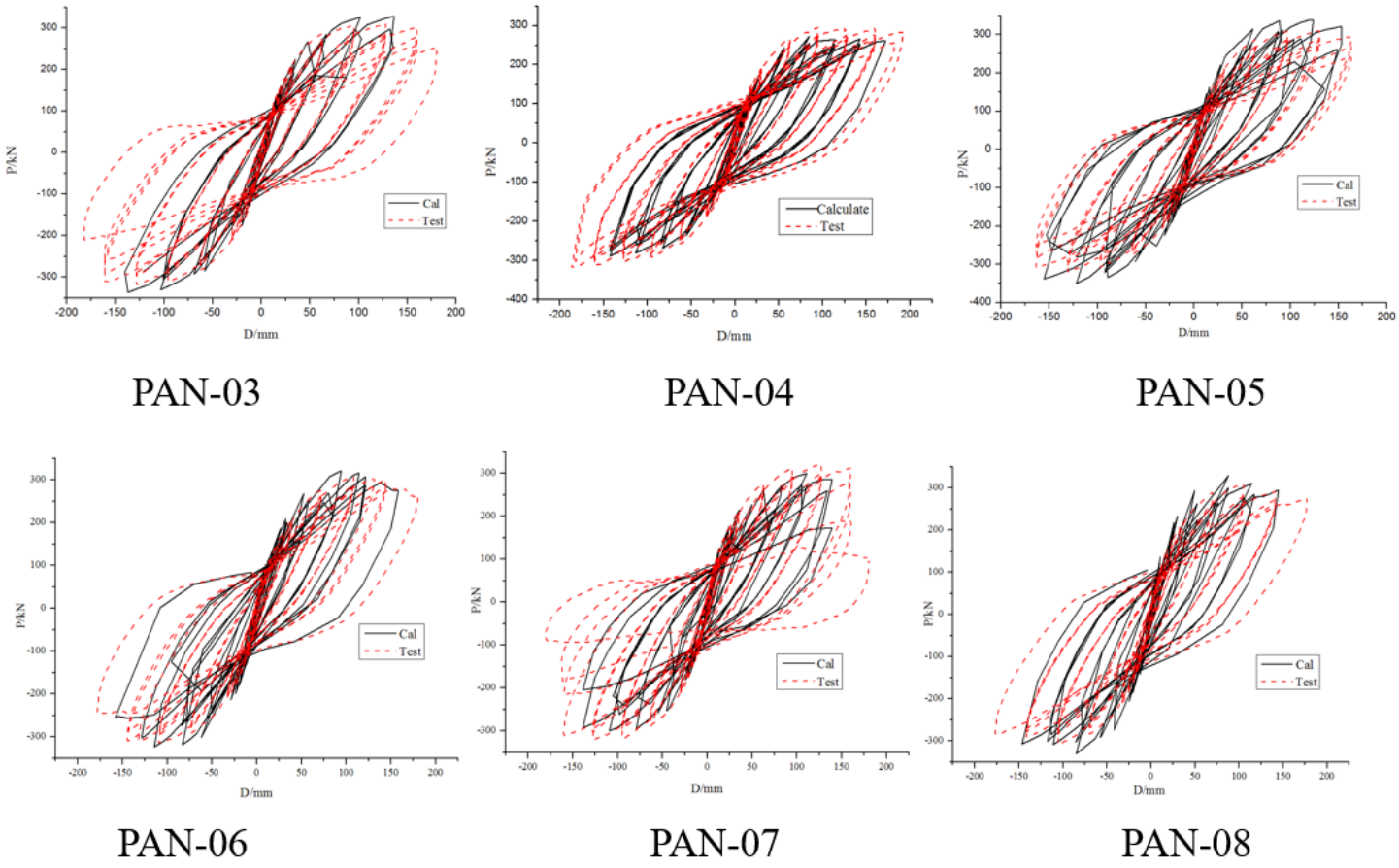

Figure 9

Comparison of results